

## Self-accelerated Corrosion of Nuclear Waste Forms at Material Interfaces

Xiaolei Guo,<sup>1</sup> Stephane Gin,<sup>2</sup> Penghui Lei,<sup>3</sup> Tiankai Yao,<sup>3</sup> Hongshen Liu,<sup>4</sup> Daniel K. Schreiber,<sup>5</sup> Dien Ngo,<sup>4</sup> Gopal Viswanathan,<sup>1</sup> Tianshu Li,<sup>1</sup> Seong H. Kim,<sup>4</sup> John D. Vienna,<sup>5</sup> Joseph V. Ryan,<sup>5</sup> Jincheng Du,<sup>6</sup> Jie Lian,<sup>3</sup> Gerald S. Frankel<sup>1\*</sup>

<sup>1</sup>*Department of Materials Science and Engineering, Ohio State University, Columbus, OH 43210, USA*

<sup>2</sup>*CEA, DEN, DE2D, SEVT, F-30207 Bagnols sur Cèze, France*

<sup>3</sup>*Department of Mechanical Aerospace and Nuclear Engineering, Rensselaer Polytechnic Institute, Troy, NY 12180*

<sup>4</sup>*Department of Chemical Engineering and Materials Research Institute, Pennsylvania State University, University Park, PA 16802, USA*

<sup>5</sup>*Energy and Environment Directorate, Pacific Northwest National Laboratory, Richland, WA 99352, USA*

<sup>6</sup>*Department of Materials Science and Engineering, University of North Texas, Denton, TX 76203, USA*

### Abstract

The U.S. plan for high-level nuclear waste includes immobilization of long-lived radionuclides in glass or ceramic waste forms in stainless steel (SS) canisters for disposal in deep geological repositories. Here we report that, under simulated repository conditions, corrosion could be significantly accelerated at the interfaces of different barrier materials, which has not been considered in the current safety and performance assessment models. Severe localized corrosion was found at the interfaces between SS and a model nuclear waste glass and between SS and a ceramic waste form. The accelerated corrosion can be attributed to changes of solution chemistry and local acidity/alkalinity within a confined space, which significantly alter the corrosion of both the waste form materials and metallic canisters. The corrosion that is accelerated by the interface interaction between dissimilar materials could profoundly impact the service life of the nuclear waste packages, which, therefore, should be carefully considered when evaluating the performance of waste forms and their packages. Moreover, compatible barriers should be selected to further optimize the performance of the geological repository system.

Nuclear waste disposal is a complicated problem that requires utilization of different classes of materials, including metals, crystalline ceramics, and glass. Nearly all nations that reprocess irradiated nuclear fuels have adopted deep geological disposal to isolate the resulting high-level nuclear waste (HLW), which will remain hazardous to humans and the environment for hundreds of thousands of years. In this plan, the HLW will primarily be melted together with other additives to form borosilicate waste glass, and then cast into stainless steel (SS) canisters<sup>1</sup>. Wastes containing problematic radionuclides such as long-lived and semi-volatile I-129 and Tc-99 might be isolated in crystalline ceramic waste forms and then also enclosed in metallic canisters. As a result, there will inevitably be interfaces between the SS canister and the glass or ceramic waste forms. During long-time exposure in the repository, after a cooling period, an aqueous environment could exist outside the waste packages<sup>2</sup>, and it is possible that the metallic canisters could be breached by pitting corrosion<sup>3</sup>, allowing the corrosive electrolyte to reach the encapsulated glass or ceramic waste forms, which can eventually lead to their alteration and release of radionuclides. When the electrolyte penetrates the interfaces between metal and glass or ceramics, another localized corrosion phenomenon, crevice corrosion, could be triggered<sup>4</sup>.

A schematic illustration of the potential metal crevice corrosion event after the canister is breached is shown in **Fig. 1**: when SS is partially shielded from the environment by glass or ceramics, a confined crevice space is created at the interface where initially both anodic (metal dissolution) and cathodic (oxygen reduction reaction, ORR) reactions occur simultaneously. Due to mass transport limitations, oxygen is quickly depleted inside the crevice, after which the dominant reaction within the crevice will be metal dissolution. These reactions create an extremely aggressive environment that is enriched in metal cations. These metal cations will hydrolyze and drastically increase the local acidity within the confined space<sup>4</sup>, altering the corrosion and degradation behavior of both the waste form materials and the metal canister. The enhancement of metal corrosion due to its own corrosion products can be considered a self-acceleration effect. In addition, the ORR will strongly increase the pH near the cathodes, which could

have a substantial impact on the precipitation of secondary phases, and thus influence the long-term durability of nuclear waste forms. Owing to the inhomogeneous current distribution and resulting ohmic potential drop, the corrosion attack is generally localized near the crevice mouth area, creating what will hereafter be referred to as crevice corrosion characteristics. Since such crevice damage is localized, it may cause accelerated failure of the SS canister, and thus expose more glass or ceramic waste forms to the environment. However, the current safety and performance evaluation models are derived from data obtained from individual material groups, i.e. the glass or ceramic waste forms or the metallic containers. Little attention has been paid to the potential interactions between different materials when they are brought together as a repository system. In this report, we demonstrate that corrosion could be significantly accelerated at the interfaces between the metal canister and waste forms due to the local chemistry changes.

To investigate the impact of the interface interaction on corrosion of a waste package, dissimilar waste form materials were pressed against each other and corroded at 90 °C in 0.6 M NaCl solutions for up to 30 days, simulating corrosion under repository conditions. More experimental details are included in the supplementary materials. The Cl<sup>-</sup> anion concentration will be much lower for a repository exposed to ground water, probably several mM<sup>5</sup>. However, the Cl<sup>-</sup> ions will be enriched in the confined material interfaces owing to crevice corrosion<sup>4</sup>. Meanwhile, the leaching of glass is also likely to supply abundant alkali cations such as Na<sup>+</sup>. Therefore, the 0.6 M NaCl solution used here is a reasonable surrogate for the actual disposal conditions, which are not exactly known at this point. While many countries are considering anoxic repository environments, this study was performed under oxic conditions, which is relevant to U.S. Yucca Mountain project<sup>6</sup>. SS316 with primary composition 17Cr-12Ni-2.5Mo-balFe (wt.%) was used as a representative canister material in this study. The glass used here is a simplified model nuclear waste glass called international simple glass (ISG)<sup>1</sup>, which contains 60.2SiO<sub>2</sub>-16.0B<sub>2</sub>O<sub>3</sub>-12.6Na<sub>2</sub>O-3.8Al<sub>2</sub>O<sub>3</sub>-5.7CaO-1.7ZrO<sub>2</sub> (mol%). Dense ceramic pellets of Ba<sub>1.15</sub>(Cl/Al)<sub>2.3</sub>Ti<sub>5.7</sub>O<sub>16</sub> in a hollandite structure for potential Cs incorporation were used as the model system for studying

metal/ceramic interactions. We present below evidence that both glass and crystalline ceramic corrosion could be strongly affected by the metal crevice environment at the interface of dissimilar materials.

As shown in **Fig. 2a**, when SS was corroded in close proximity to ISG, severe localized corrosion occurred along the boundary of the SS/ISG contact area. Crevice corrosion characteristics were also observed on the ISG surface that was corroded in direct contact with SS (denoted as ISG(+SS)), where localized corrosion was found in the crevice mouth area, but the center of the crevice was less altered (**Fig. 2b**). Upon drying of the ISG in air, cracking of the glass gel layer could only be observed in the crevice mouth area (**Fig. 2c**). X-ray photoelectron spectroscopy (XPS) analysis of the glass surface (**Fig. 2e**) showed that the crevice mouth area was depleted in all glass components except for Si, suggesting a corrosion mechanism that is typical for glass in acidic solutions<sup>7</sup>. Meanwhile, a substantial amount of Fe was detected in this area, which could only have originated from corrosion of the SS. Scanning electron microscopy (SEM) identified a heterogeneous alteration (gel) layer on the glass surface (**Fig. 2d**). The gel thickness was approximately 30  $\mu\text{m}$  in the crevice mouth area, and it decreased gradually along the crevice center direction. In comparison, a gel layer with a constant thickness also formed on a control test sample made by contact with polytetrafluoroethylene (PTFE), denoted as ISG(+PTFE), but the maximum thickness was only about 15  $\mu\text{m}$  (Fig. S1). This suggests that ISG corrosion was accelerated when in contact with SS. Time-of-Flight Secondary Ion Mass Spectrometry (ToF-SIMS) elemental mapping identified Fe and Cr in the gel layer, as well as in the outermost layer of the pristine glass (Fig. S2). The presence of Fe-silicate species has been known to retard the formation of the passivation layer of borosilicate glass and thus enhance the residual glass corrosion rate<sup>8,9</sup>. As Cr could substitute for Fe in clay-type minerals, it can be assumed that both Fe and Cr could have an adverse effect on glass durability. Therefore, the affinity of Fe and Cr for Si could have an adverse effect on glass durability. In contrast, no localized crevice corrosion characteristics were identified on an ISG(+PTFE) surface (**Fig. 2b''**). Instead, a random corrosion morphology was observed across the entire surface, suggesting that what was

observed in **Fig. 2b** could not be simply attributed to the high surface to solution volume ratio in the crevice.

It is apparent that the presence of a SS crevice significantly enhanced the ISG corrosion. Correspondingly, ISG influenced the extent of SS localized corrosion, in fact reducing it. As shown in **Fig. 3a**, multiple corrosion pits were observed on SS when in contact with ISG, SS(+ISG). However, when SS was corroded in close proximity to PTFE, more severe pitting damage was found on the SS surface, as shown in **Fig. 3b**. SEM revealed the existence of a deposited film across the entire surface of SS(+ISG) (**Fig. 3c-3d**). XPS analysis suggested that the film was primarily enriched in Fe and silica (**Fig. 3e**). Scanning transmission electron microscopy and energy-dispersive X-ray spectroscopy (STEM/EDS) (**Fig. 3f**) analysis on the cross-section of the film further confirmed that the film consists of Si, Al, Na, Ca, and Zr, which originated from the ISG, and Fe, Ni, and Cr from SS corrosion. Zr is generally considered as an immobile element during glass corrosion owing to the low solubility of Zr hydrous oxides between pH 3 and 11<sup>10,11</sup>, so the presence of Zr in the precipitated film further validates acidic glass corrosion within the crevice. Because Zr has been known to reduce glass corrosion rates by immobilizing neighboring atoms<sup>12</sup>, its release from the ISG also suggests that the gel on the ISG is not protective. In regions outside of the crevice, a substantial amount of secondary phase particles were identified (**Fig. 4a**). STEM (**Fig. 4b-4c**) and EDS (**Fig. 4d-4e**) analysis revealed that the precipitated particles consist of multiple crystalline phases, including a cuboidal Fe-silicate phase (**Fig. 4b**, phase 1), a needle-shaped Si- and Al-rich zeolite phase that is likely flörkeite (**Fig. 4b**, phase 2, Table S5), another Si- and Al- rich zeolite-like phase with different composition and morphology (**Fig. 4c**, phase 3), and a titanium oxide phase originated from SS corrosion (**Fig. 4c**, phase 4). These crystalline phases were embedded in a large amorphous matrix enriched in Si. The nucleation and growth of these Si-rich minerals, along with the precipitation of continuous film observed in **Fig. 3c-f**, will consume silicates from solution, promoting further glass dissolution, and ultimately accelerating overall glass corrosion similarly to stage III behavior of glass corrosion<sup>13</sup>. The precipitation of zeolite-type minerals has not been observed in glass corrosion studies

under conditions with  $\text{pH} < 10^{14}$ . However, in this study, such particles were observed in a bulk solution with pH of 8.3. This is probably due to the ORR at the cathodic area of SS, which generated  $\text{OH}^-$  ions and increased the local alkalinity. The formation of such phases at a much lower bulk pH value than previously thought possible suggests that SS corrosion could have a profound impact on the long-term durability of nuclear glass by triggering the accelerated stage III.

Various ceramic waste forms have been proposed to immobilize semi-volatile and/or long-lived radionuclides. However, the criteria for selecting such materials have not included the potential impact of the interaction between the ceramic and metallic canister corrosion. We demonstrate below that the interactions between ceramics and metals could lead to severe localized corrosion of both materials. Two titanate based ceramic waste forms,  $\text{Ba}_{1.15}\text{Cr}_{2.3}\text{Ti}_{5.7}\text{O}_{16}$  hollandite and  $\text{Ba}_{1.15}\text{Al}_{2.3}\text{Ti}_{5.7}\text{O}_{16}$  hollandite<sup>15</sup>, hereafter referred to as Cr-Hol and Al-Hol, respectively, are used as examples. Deep pits were observed on SS after only 28 days of corrosion in close proximity to Cr-Hol (**Fig. 5a-5c**). Small pits were found in the crevice mouth area, while large pits were present in the crevice center. In contrast, when a similar experiment was conducted by pressing SS against Al-Hol, where Cr was replaced by Al, no localized damage was found on the SS surface (Fig. S3). The crevice corrosion susceptibility of metals is typically studied by pressing them against a ceramic or polymer (e.g., PTFE) crevice former<sup>16</sup>, as these materials are considered chemically “inert”. However, as demonstrated in this study, the corrosion of SS could be strongly affected by contact with certain ceramic waste forms.

In a typical crevice corrosion experiment in which SS is pressed against PTFE, the SS is the only source of dissolved cations including  $\text{Fe}^{2+}$ ,  $\text{Ni}^{2+}$ ,  $\text{Cr}^{3+}$ , and  $\text{Mo}^{3+}$ . Under anodic control, the rate of cations released from SS is determined by the metal passive current density, which is often smaller than  $1 \mu\text{A}/\text{cm}^2$ . In other words, although the cations can be gradually released into the crevice during corrosion, the rate is initially quite low. Due to mass transport limitations inside the crevice, the cations can accumulate within the crevice over time and hydrolyze to increase the local acidity. Additionally, the accumulation of cations will increase the local concentration of aggressive anions, such as  $\text{Cl}^-$ , by electro-

migration to maintain charge neutrality of the crevice solution. Among the cations generated by SS corrosion,  $\text{Cr}^{3+}$  has the largest hydrolysis constant, and the solubility of its hydroxide is the lowest (insoluble even in acidic conditions)<sup>4</sup>. As a result, the rate of pH drop and the accumulation of aggressive anions within the crevice strongly depend on the local concentration of  $\text{Cr}^{3+}$ . When the concentration of cations reaches a critical value, the protective passive film on the SS surface will break down, which triggers the onset of rapid localized corrosion<sup>17</sup>. This process is usually assisted by the attack of  $\text{Cl}^-$  ions. When Cr-Hol is present near SS, it could serve as another source of  $\text{Cr}^{3+}$  ions. Therefore, the leaching of  $\text{Cr}^{3+}$  from the hollandite could shorten the incubation time required to accumulate sufficient  $\text{Cr}^{3+}$  ions within the crevice, and thus accelerate the SS crevice corrosion. As shown in **Fig. 5d**, STEM high-angle annular dark-field imaging (HAADF) and EDS elemental mapping of the corroded hollandite cross-section revealed that Cr was depleted from the surface, leaving behind a Ti-enriched matrix. The surface was also covered by a Mo rich film that originated from SS corrosion. Secondary phase particles enriched in Fe, Ni, and Cr oxide, which are also derived from SS corrosion, are present on top of the Mo rich film. The distribution of these different phases suggests that  $\text{Cr}^{3+}$  leached from hollandite prior to the severe corrosion of SS, which further supports the notion that it was the cause and not an effect. In comparison, although the leaching rate of  $\text{Al}^{3+}$  from the hollandite is higher than  $\text{Cr}^{3+}$  (Fig. S4), its hydrolysis constant is much lower compared to  $\text{Cr}^{3+4}$ , which explains the drastically different corrosion morphologies between SS/Cr-Hol and SS/Al-Hol.

The leaching rate of  $\text{Cr}^{3+}$  from Cr-Hol decreases over time (Fig. S4), but the release of  $\text{Cr}^{3+}$  due to SS crevice corrosion is self-accelerating in nature, owing to the separation of the anode and cathode. Therefore, SS crevice corrosion could have a significant impact on hollandite corrosion by increasing the local acidity. As shown in **Fig. 5e-5f**, the crevice corrosion characteristics were also observed on Cr-Hol after corroding in close proximity to SS, where the crevice mouth area was more severely attacked. However, corrosion was also observed in the central areas of Cr-Hol that were in direct contact with the large pits in the SS, which was apparently influenced by the aggressive environment created by the severe

pitting corrosion nearby (detailed mechanisms described in Supplementary Materials). The region between the crevice mouth and center was generally less corroded, probably because they were not in direct contact with pits on the SS. The morphology of the crevice mouth was similar to that of Cr-Hol corroded in HCl (pH=2) solutions (**Fig. 5g**). On the other hand, no visible corrosion was identified on Cr-Hol corroded in neutral 0.6 M NaCl solutions after 28 days, suggesting that the local environment in the crevice mouth regime was acidic. In addition, leaching data showed that Cr release rate increases as the proton concentration increases (Fig. S5). Therefore, in a confined crevice space, the corrosion rate of Cr-Hol should be significantly enhanced due to the high local acidity created by SS crevice corrosion. In practical applications, this could lead to enhanced release of radionuclides from this ceramic waste form.

In summary, when different materials are brought in direct contact in aqueous environment, their corrosion products may create feedback effects that could further influence their corrosion behaviors. The crevice corrosion of SS creates a highly acidic environment that significantly increases the localized corrosion rate of ISG placed in close proximity. Additionally, the cathodic reaction of SS increases the local alkalinity, which assists the formation of minerals that increase the glass corrosion rate at a much lower bulk pH value than previously thought possible. More importantly, the crosstalk between SS and ISG corrosion resulted in the formation of a continuous film at the interface, which drastically consumed Si and other gel formers such as Al and Zr, and thus promotes the dissolution of ISG and causes the loss of gel protectiveness. This phenomenon could induce sudden acceleration of glass corrosion and eventually lead to the higher release of radionuclides. On the other hand, ISG corrosion seems to reduce the localized corrosion of SS by the precipitation of a silicate rich surface film. However, this film did not completely suppress the corrosion of SS, which was sufficient to cause the enhanced corrosion of ISG. The fact that SS accelerates ISG corrosion while ISG suppresses SS corrosion suggests that the dominant corroding species at the SS and ISG interface are metal cations that were generated from metal dissolution. However, this does not necessarily mean that SS corrosion products were formed prior to the ISG corrosion products. Due to the self-acceleration effect of metal crevice corrosion, once the metal cations

are generated, the accumulation rate is likely much higher than that of the ISG corrosion products, which resulted in the crevice damage observed on SS and localized corrosion on ISG. Unlike the interactions between SS and ISG, the contact of SS and Cr-Hol ceramic waste form enhanced the corrosion of both materials at the interface. This could be attributed to the leaching of  $\text{Cr}^{3+}$  ions from both materials, which more quickly exceeds a threshold for SS passive film breakdown. Therefore, in general, the interfaces of metal/glass or metal/ceramics are prone to enhanced corrosion, primarily due to mass transport limitations, which could cause enhanced radionuclide releases from a nuclear waste disposal system. Although the reported experiments are for 30-day immersion, the fundamental mechanisms that have been identified can be included in predictive models to test the effects of time and other parameters. Such models exist in the literature (e.g. GRAAL model<sup>18</sup>) and have been tested over long time scales with archeological analogs<sup>19</sup>. It is thus possible to bridge the time scale gap between lab and field. While a single study cannot answer all the questions, this work paves the way for more studies that could increase the accuracy of predictive models. Apparently, the most effective approach to eliminate the interfacial damage is to completely isolate water from the disposal system, which is challenging given the unpredictability of geological environment over extremely long periods of time. For instance, after the Yucca Mountain repository is filled and closed, it will undergo one very long thermal cycle. The temperature will increase initially due to the decay heat of the waste and then cool down over time<sup>20</sup>. During the heat-up phase, water in the mountain may be driven away from the repository. However, when the repository cools, water may flow back to the canisters and dripping water is expected. The local relative humidity may eventually increase and could be above 75% after 1000 years<sup>20</sup>. Considering that the repository lifetime is typically described to be >100,000 years, the dry hot stage will be only a small percentage. Most of the lifetime of the repository will be relatively cool and humid, with the possibility of dripping water. Therefore, similar to all current performance assessment models, it must be assumed that water will eventually reach the immobilized waste. Current models must be improved by incorporating the potential synergistic corrosion behavior at the interfaces of dissimilar materials to avoid the underestimation of corrosion damage. Moreover, the compatibility of different barriers should be carefully examined and

may be optimized, especially the hydrolysis of ions that may be released and accumulated at the materials interfaces.

## References

- 1 Gin, S. *et al.* An international initiative on long-term behavior of high-level nuclear waste glass. *Materials Today* **16**, 243-248 (2013).
- 2 Bates, J., Bradley, J., Teetsov, A., Bradley, C. & Ten Brink, M. B. Colloid formation during waste form reaction: implications for nuclear waste disposal. *Science* **256**, 649-651 (1992).
- 3 Frankel, G. Pitting corrosion of metals a review of the critical factors. *Journal of the Electrochemical Society* **145**, 2186-2198 (1998).
- 4 Oldfield, J. & Sutton, W. Crevice corrosion of stainless steels: i. a mathematical model. *British corrosion journal* **13**, 13-22 (1978).
- 5 Rydberg, J. Groundwater chemistry of a nuclear waste repository in granite bedrock. (Lawrence Livermore National Lab., CA (USA), 1981).
- 6 Long, J. C. & Ewing, R. C. Yucca Mountain: Earth-science issues at a geologic repository for high-level nuclear waste. *Annu. Rev. Earth Planet. Sci.* **32**, 363-401 (2004).
- 7 Geisler, T. *et al.* Aqueous corrosion of borosilicate glass under acidic conditions: a new corrosion mechanism. *Journal of Non-Crystalline Solids* **356**, 1458-1465 (2010).
- 8 McVAY, G. L. & BUCKWALTER, C. Q. Effect of iron on waste-glass leaching. *Journal of the American Ceramic Society* **66**, 170-174 (1983).
- 9 Burger, E. *et al.* Impact of iron on nuclear glass alteration in geological repository conditions: A multiscale approach. *Applied geochemistry* **31**, 159-170 (2013).
- 10 Pourbaix, M. Atlas of electrochemical equilibria in aqueous solution. *NACE* **307** (1974).
- 11 Brendebach, B., Altmaier, M., Rothe, J., Neck, V. & Denecke, M. EXAFS study of aqueous ZrIV and ThIV complexes in alkaline CaCl<sub>2</sub> solutions: Ca<sub>3</sub> [Zr (OH) 6] 4+ and Ca<sub>4</sub> [Th (OH) 8] 4+. *Inorganic chemistry* **46**, 6804-6810 (2007).
- 12 Arab, M. *et al.* Aqueous alteration of five-oxide silicate glasses: experimental approach and Monte Carlo modeling. *Journal of Non-Crystalline Solids* **354**, 155-161 (2008).
- 13 Fournier, M., Gin, S., Frugier, P. & Mercado-Depierre, S. Contribution of zeolite-seeded experiments to the understanding of resumption of glass alteration. *npj Materials Degradation* **1**, 17 (2017).
- 14 Fournier, M., Frugier, P. & Gin, S. Effect of zeolite formation on borosilicate glass dissolution kinetics. *Procedia Earth and Planetary Science* **7**, 264-267 (2013).
- 15 Ringwood, A., Kesson, S., Ware, N., Hibberson, W. & Major, A. Immobilisation of high level nuclear reactor wastes in SYNROC. *Nature* **278**, 219 (1979).
- 16 Shan, X. & Payer, J. H. Comparison of Ceramic and Polymer Crevice Formers on the Crevice Corrosion Behavior of Ni-Cr-Mo Alloy C-22. in *CORROSION 2007*. (NACE International).
- 17 Li, T., Scully, J. & Frankel, G. Localized Corrosion: Passive Film Breakdown vs. Pit Growth Stability: Part III. A Unifying Set of Principal Parameters and Criteria for Pit Stabilization and Salt Film Formation. *Journal of The Electrochemical Society* **165**, C762-C770 (2018).
- 18 Frugier, P., Minet, Y., Rajmohan, N., Godon, N. & Gin, S. Modeling glass corrosion with GRAAL. *npj Materials Degradation* **2**, 35, doi:10.1038/s41529-018-0056-z (2018).
- 19 Verney-Carron, A., Gin, S. & Libourel, G. Archaeological analogs and the future of nuclear waste glass. *J Nucl Mater* **406**, 365-370, doi:https://doi.org/10.1016/j.jnucmat.2010.09.028 (2010).
- 20 Payer, J. H., Carroll, S. A., Gdowski, G. E. & Rebak, R. B. A Framework for the Analysis of Localized Corrosion at the Proposed Yucca Mountain Repository. (Yucca Mountain Project, Las Vegas, Nevada, 2006).

## Methods

### Materials

International simple glass (ISG) samples were provided by Pacific Northwest National Laboratory and Savannah River National Laboratory. The nominal composition of ISG is listed in Table S1<sup>1,21</sup>. Stainless steel (SS) 316 (UNS S31600) was purchased from McMaster-Carr with nominal composition shown in Table S2. All water used in this study was deionized water (DI water) with a minimum electrical resistivity of 18 M $\Omega$ ·cm (ASTM Type I water). Perfluoroalkoxy alkane (PFA) vessels and Teflon<sup>TM</sup> coupons/tapes were pretreated with NaOH and DI water to remove fluoride ions before use<sup>22</sup>. Sodium chloride (NaCl) (crystalline/certified ACS, CAT# S27150) was purchased from Fisher Scientific and used without further modification/purification.

### Synthesis of Hollandite Ceramic Samples

Hollandite ceramic waste forms of the compositions Ba<sub>1.15</sub>M<sup>3+</sup><sub>2.3</sub>Ti<sub>5.7</sub>O<sub>16</sub>, (M = Al or Cr) were synthesized via solid-state reactions. Ba(NO<sub>3</sub>)<sub>2</sub>, Cr<sub>2</sub>O<sub>3</sub>, and Al<sub>2</sub>O<sub>3</sub> were used as the precursors, which were mixed in stoichiometric ratios and homogenized in a high-energy ball-mill system. Approximately 10 grams of starting materials were ground using 1 mm Zr balls in ethanol at 500 rpm for 10 cycles. Each cycle consisted of 15 min of grinding time and 5 min of cooling time. The resultant mixture was dried, and calcinated at 600 °C for 4 h to decompose the nitrates. The calcinated powders were compressed into pellets with diameter of 10 mm before sintering. The sintering of Ba<sub>1.15</sub>Cr<sub>2.3</sub>Ti<sub>5.7</sub>O<sub>16</sub> (hereafter referred to as Cr-Hol) was performed at 1100 °C for 6 h, while the Ba<sub>1.15</sub>Al<sub>2.3</sub>Ti<sub>5.7</sub>O<sub>16</sub> (hereafter referred to as Al-Hol) was sintered at 1200 °C for 24 h. After sintering, the pellets were ground by hand, and consolidated using a spark-plasma sintering (SPS) approach (Dr. Sinter® SPS-211 Lx system) under a constant flow of Ar gas. The system was heated rapidly to 600 °C under an initial pressure of 10 MPa. And then the temperature and pressure were further increased at a rate of 50 °C/min and 5 MPa/min, respectively, until reaching a peak temperature of 1300 °C and a peak pressure of 40 MPa. After maintaining the peak

temperature and pressure for additional 10 min, the pressure was released, and the samples were cooled down to room temperature in an Ar atmosphere.

### **Corrosion of ISG/SS**

An ISG block was cut into coupons with dimensions of 25 mm × 13 mm × 3 mm and abraded to 1200 grit using SiC paper. A SS sheet was cut into 25 mm × 25 mm × 3 mm coupons and abraded to 600 grit with SiC paper for further usage. After extensive rinsing in ethanol and then DI water, the SS was placed on top of the ISG to form a crevice space between them. Both SS and ISG specimens were wetted with 0.6 M NaCl solution before they were placed in contact with each other. The gap between the two materials was only determined by the roughness of the two surfaces in contact. The assembly was wrapped with Teflon™ tape and then placed in a PFA vessel pre-filled with 0.6 M NaCl solution at 90 °C. Each PFA vessel had two open holes on the lid to enable ingress of oxygen from the ambient air, which is critical for the cathodic reactions on SS. The vessels were placed in a 90 °C water bath for the entire corrosion period. Every 2-3 days, DI water was added to the solution to compensate for evaporation. As control experiments, PTFE coupons were pressed against ISG or SS to form similar assemblies as SS/ISG, and were corroded under the same testing conditions. After 30 days of exposure, the SS/ISG, SS/PTFE, and ISG/PTFE assemblies were removed from the solutions at the same time. The harvested samples were divided into two groups. For the first group, each coupon was separated from the assembly and rinsed extensively with DI water, air dried, and stored at room temperature in a desiccator for further analysis. For the other group, the whole assemblies were cleaned with DI water and then rapidly immersed into epoxy without being separated to preserve the original features of the material interfaces. The epoxy-mounted samples were allowed to dry at room temperature overnight, and then cut in the middle to expose the cross-sections of the material interfaces. The cross-sections of epoxy mounted SS/ISG samples were abraded to 1200 grit using SiC papers and rinsed with abundant DI water and ethanol to remove the potential containments from the abrasion. The resultant samples were dried and stored at room

temperature in a desiccator for further analysis. A complete list of experimental groups has been summarized in Table S4.

### **Corrosion of SS/Hollandite**

Cr-Hol and Al-Hol pellets with diameters of 10 mm were abraded to 1200 grit using SiC papers. Similar to SS/ISG corrosion, the hollandite samples were pressed against SS coupons (25 mm × 25 mm × 3 mm) and wrapped with Teflon™ tape, and then placed in a PFA vessel pre-filled with 0.6 M NaCl solution at 90 °C. Both SS and hollandite specimens were wetted with 0.6 M NaCl solution before they were placed in contact with each other. Every 2-3 days, DI water was added to the solution to compensate for the evaporation. After 28 days of exposure, the hollandite/SS assemblies were removed from the solutions. Each material was separated from the assembly and rinsed extensively with DI water, air dried, and stored at room temperature in a desiccator for further analysis.

### **Optical Profilometry Measurement**

Optical profilometry (Bruker™) was used to characterize the topography of as-abraded SS and ISG, as well as the SS(+Cr-Hol<sub>NaCl</sub>) after 30 days of corrosion. The data were analyzed using Vision64 Software.

### **Leaching Test for Hollandite**

Leaching experiments were performed to evaluate the chemical durability of Cr-Hol and Al-Hol under neutral and acidic conditions. Prior to the test, the hollandite samples were abraded to 1 μm surface finish and then cleaned with abundant DI water. The samples were placed in PTFE containers filled with DI water or 0.01 M HCl solution, with sample surface area to volume ratio of 5 m<sup>-1</sup>. The PTFE containers were kept in an oven with temperature adjusted to 90 °C. The leachant was replaced at preset time intervals. The collected solutions were subjected to cation analysis by Inductively Coupled Plasma Mass Spectrometry (ICP-MS).

### **X-ray Photoelectron Spectroscopy (XPS) Analysis**

The corroded ISG and SS samples were subjected to XPS analysis. A PHI VersaProbe II spectrometer (Chanhasen, MN) equipped with a monochromatic Al-K $\alpha$  (1486.6 eV) X-ray source was used to analyze the glass samples. To acquire the elemental composition of the samples, survey scans and high-resolution narrow scans of the O 1s, Na KLL, Ca 2p, B 1s, Zr 3d, C 1s, Si 2p and Al 2p peaks were conducted at 187 and 117 eV pass energies, respectively, at three random locations for each sample. The SS samples were characterized using a Kratos XPS system using monochromatic Al-K $\alpha$  X-ray excitation source (12 kV, 10 mA). All spectra were referenced to the adventitious alkyl (C-C) peak with a binding energy of 285.0 eV. High-resolution C 1s core level spectra were collected at a 29 eV pass energy for peak deconvolution into alkyl (C-H), alcoholic (C-OH), carbonyl (C=O), carboxyl (O-C=O), and carbonate (CO $_3^{2-}$ ) components. Fitting of the C 1s peak was accomplished by using the Voigt function (65% Gaussian, 35% Lorentzian). The glass composition was calculated after accounting for the adventitious hydrocarbon contamination layer on the glass surface<sup>23</sup>.

### **Time-of-Flight Secondary Ion Mass Spectrometry (ToF-SIMS) analysis**

The cross-section of epoxy mounted SS-ISG samples was characterized by ToF-SIMS. A positive mode surface mapping was performed after oxygen ion cleaning (O $_2$  2k eV, 600nA, 500  $\mu\text{m} \times 500 \mu\text{m}$ , 30 seconds). The chemical maps were acquired by using 25 keV Bi $^{3+}$  primary ions in the burst mode. The analyzed area was 300  $\mu\text{m} \times 300 \mu\text{m}$  (256  $\times$  256 pixels). Neutralization of the surface was conducted by pulsed flow of electrons at low energy (<20 eV).

### **STEM-HAADF and EDS Elemental Mapping**

A foil with a thickness less than 200 nm was prepared from an SS(+ISG) sample, by a focused ion beam (FIB) system (Thermo Fisher Scientific Helios NanoLab 600 DualBeam, Thermo Fisher Scientific, Hillsboro, OR, USA). The SS was corroded in close proximity to ISG in 0.6 M NaCl solution at 90 °C for 30 days. The FIB removal was performed at a location where a secondary phase particle and a surface film were precipitated on the SS surface, which were located outside of the crevice region. The lift-out

site was chosen to sample both the particle and film. STEM/EDS characterization was performed at 300 kV on a Thermo Fisher Scientific Image-Corrected Titan3 G2 60-300 S/TEM. The S/TEM with a Super-X detector utilizing the Bruker Esprit software. The Super-X EDX detection system uses four silicon drift detectors that are located radially around the objective pole piece and specimen stage for improved collection performance. The electron diffraction patterns were collected at 300 kV on a Thermo Fisher Scientific TECNAI G2 30 TEM. Limited sets of diffraction patterns were obtained from the needle-shaped phase shown in **Fig. 4b** (phase 2) by tilting the TEM sample holder at multiple  $\alpha$  and  $\beta$  angles. The d spacing values were extracted and listed in Table S5 along with the corresponding Miller indices. A low amount of Mg was observed (**Fig. 4e**) during the EDS analysis, which was likely from the impurity of the ISG sample.

For Cr-Hol, the lift-out lamella sample with a thickness around 100 nm was prepared by a FIB system (Thermo Fisher Scientific, Quanta 3D FEG, Thermo Fisher Scientific, Hillsboro, OR, USA) at a site on the corroded Cr-Hol surface corresponding to a pitting location where the corrosion of SS316 was significantly accelerated. At this site, the Cr-Hol surface was flat and covered by a continuous film with particles. The lift-out site was chosen to sample both the film and particle. STEM characterization was carried out using a Thermo Fisher Scientific Titan 80-300 monochromated S/TEM. The S/TEM operated at an accelerated voltage of 300-kV. A beam current of 0.5-nA with a dwell time of 15  $\mu$ s on each pixel was maintained during elementary analysis using a Super-X EDS tool inside the Titan.

## **Acknowledgment**

This work was supported as part of the Center for Performance and Design of Nuclear Waste Forms and Containers, an Energy Frontier Research Center funded by the U.S. Department of Energy, Office of Science, Basic Energy Sciences under Award # DESC0016584. The authors would like to thank Dr. Charles Crawford for supplying the International Simple Glass. The authors are grateful to Dr. Steven

Boona and Dr. Elizabeth L. Alexander from Ohio State University, and Dr. Laurent Dupuy from TESCOAN Analytics, and Drs. Matthew.J. Olszta, Nicole Overman from PNNL for the technical support.

### **Author Contributions**

X.G., S.G., J.L., S.K., J.D.V., J.V.R., J.D., and G.S.F designed the research; X.G., P.L. Y.T., H.L., D.K.S. D.N. G.V. performed the research; X.G., S.G., P.L., T.Y., H.L., D.K.S., D.N., S.K. analyzed the data. All authors contributed to the editing of the paper, and approval of the content in its current form.

### **Data Availability**

The data that support the findings of this study are available from the corresponding authors on reasonable request.

### **Competing Interests Statement**

The authors declare no competing financial interests.

## References

- 1 Gin, S. *et al.* An international initiative on long-term behavior of high-level nuclear waste glass. *Materials Today* **16**, 243-248 (2013).
- 21 Gin, S. *et al.* The fate of silicon during glass corrosion under alkaline conditions: a mechanistic and kinetic study with the international simple glass. *Geochimica et Cosmochimica Acta* **151**, 68-85 (2015).
- 22 Jantzen, C. M. & Bibler, N. E. The Product Consistency Test (ASTM C1285) for Waste Form Durability Testing. in *Environmental Issues and Waste Management Technologies in the Ceramic and Nuclear Industries XI: Proceedings of the 107th Annual Meeting of The American Ceramic Society, Baltimore, Maryland, USA 2005, Ceramic Transactions*. 141(Wiley-American Ceramic Society).
- 23 Smith, G. C. Evaluation of a simple correction for the hydrocarbon contamination layer in quantitative surface analysis by XPS. *Journal of electron spectroscopy and related phenomena* **148**, 21-28 (2005).

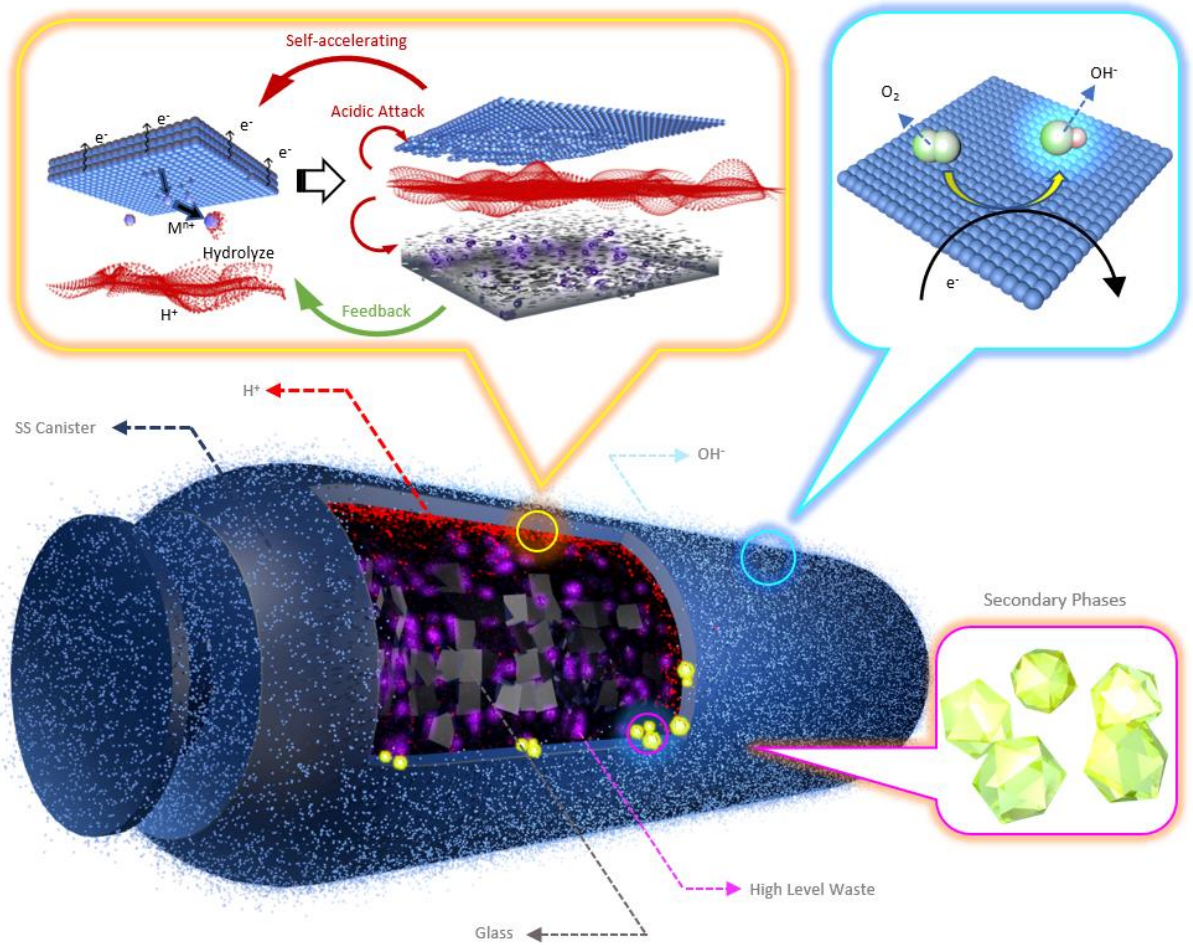


Fig. 1 Illustration of crevice corrosion for a SS canister and the potential impact on contained nuclear waste forms. High level waste (purple particles) is immobilized in glass, and then cast into a SS canister. Upon cooling, a confined crevice space will form at the SS/glass interface. Anodic dissolution of SS (blue matrix) generates metal cations, which hydrolyze to form protons (red particles) and strongly increase the local acidity. This acidic environment will further corrode the SS and glass, which leads to the release of radionuclides. Meanwhile, corrosion of glass also releases various ions that could cause feedback effect on SS corrosion. Oxygen molecules are reduced on the cathodic regions located outside of the crevice, forming hydroxide ions (glowing blue particles) that increase the local alkalinity in the exterior. The increased pH environment may trigger the precipitation of secondary phases (yellow crystals) that may be detrimental to nuclear glass durability. Dimensions are not to scale.

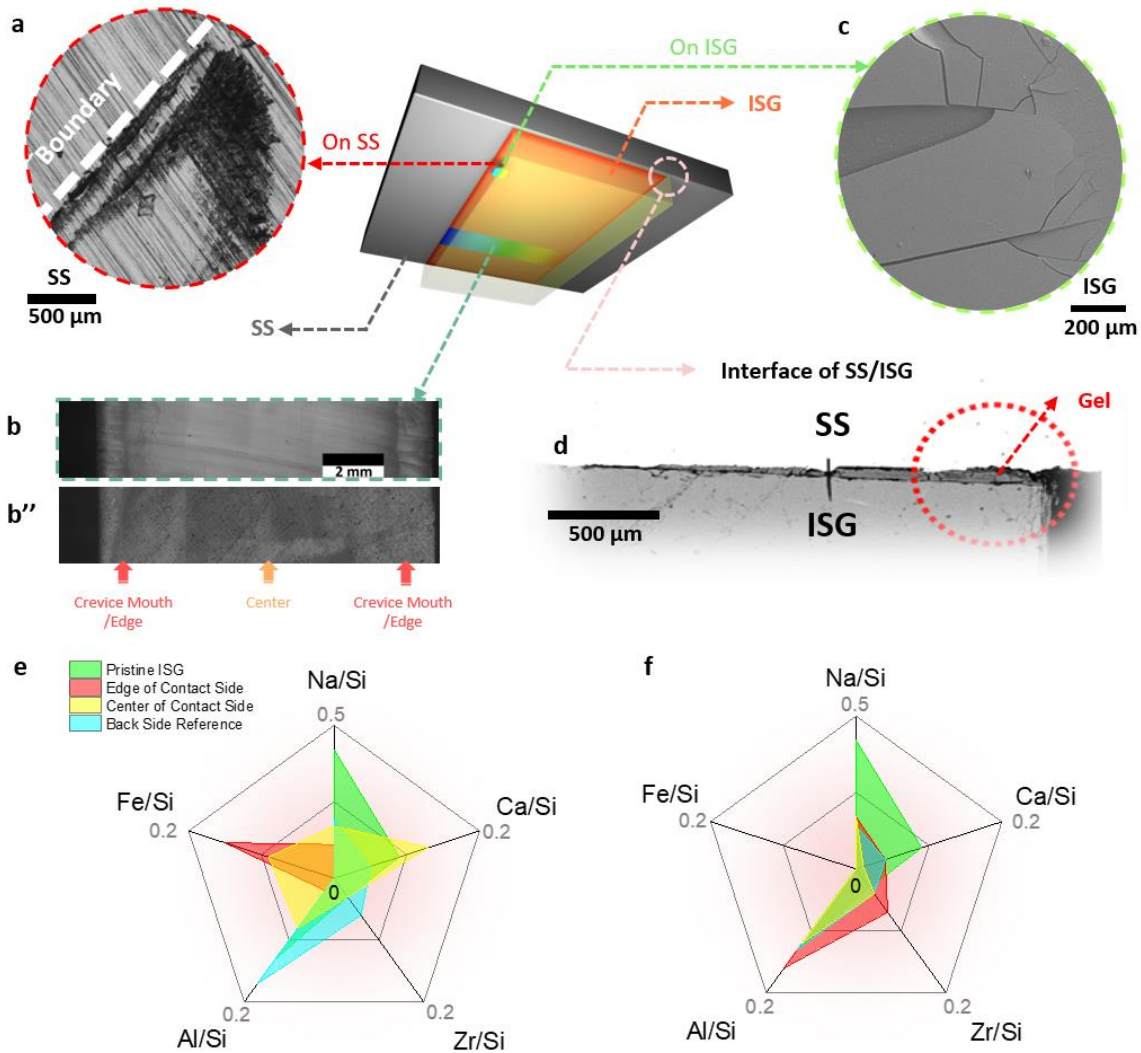


Fig. 2 Characterizations of different materials after corrosion in close proximity. a) The bottom surface of SS in contact with ISG. Severe crevice corrosion was observed on SS along the boundary of the SS/ISG contact area. b) Crevice corrosion characteristics were also observed on the ISG along the crevice boundary. b'') Random corrosion observed on the ISG that was pressed against PTFE (control group). c) The top surface of ISG facing SS. Cracks observed only in the crevice mouth area. d) Cross-section of SS/ISG interface. The red dot circle shows a thick glass gel layer formed in the crevice mouth area. Note that all samples were corroded in 0.6 M NaCl solution at 90 °C. Comparison of surface composition of ISG after being corroded in close proximity to e) SS and f) PTFE. The surface composition was quantified by XPS and normalized to the concentration of Si. \*Data also provided in Table S3.

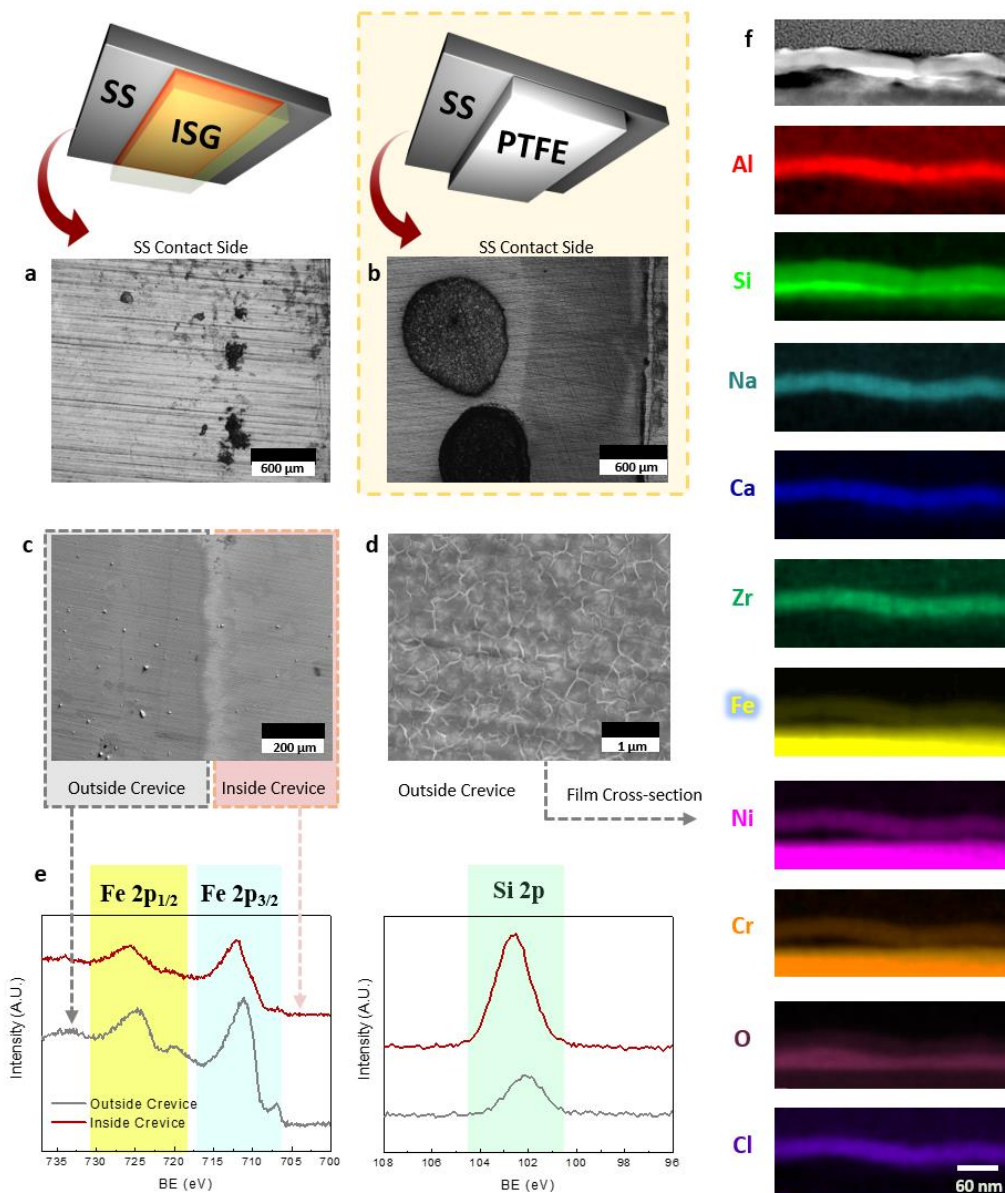


Fig. 3 Surface analysis of SS after corrosion in close proximity to ISG or PTFE. Pitting corrosion observed on a) SS pressed against ISG, and b) SS pressed against PTFE. c-d) A surface film observed on SS across the entire surface, which was more evident near the boundary of the contact area. A large number of secondary phase particles were visible outside of the crevice. e) XPS spectra obtained from SS surface corroded in close proximity to ISG. The areas inside and outside of the crevice are compared. The fitted spectra are also provided in Fig. S4. f) STEM HAADF image and EDS elemental mapping for the cross-section of the film observed in c-d).

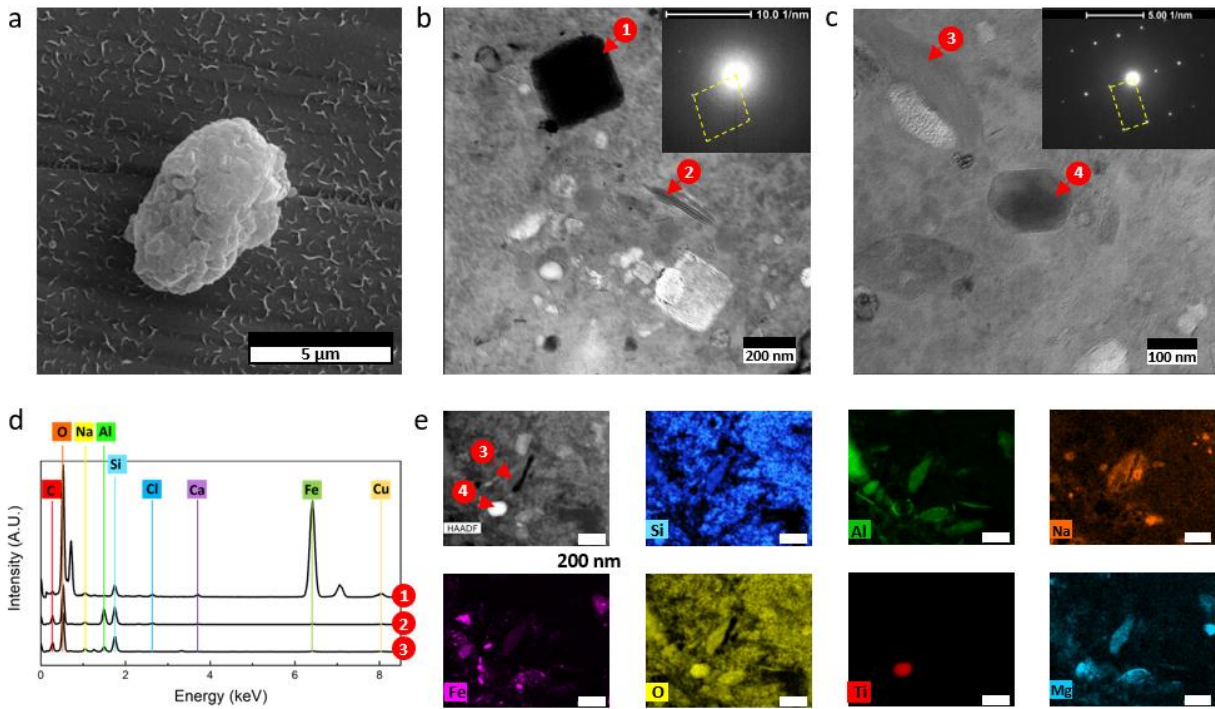


Fig. 4 Precipitation of secondary phases on SS corroded near ISG. a) Morphology of one typical particle precipitated on the surface of SS that was corroded in close proximity to ISG. b-c) TEM images of the cross-section of the particle observed in a). Four crystalline phases were highlighted: 1. a cuboidal Fe-silicate phase. 2. a needle-shaped Al- and Si- rich zeolite phase. 3. Another zeolite-like phase. 4. Titanium oxide phase originated from SS corrosion. The diffraction patterns of phase 2 and 4 were inserted in b) and c) respectively. d) The EDS spectra of phases 1-3. e) HAADF image and EDS elemental mapping for the area containing phase 3 and 4.

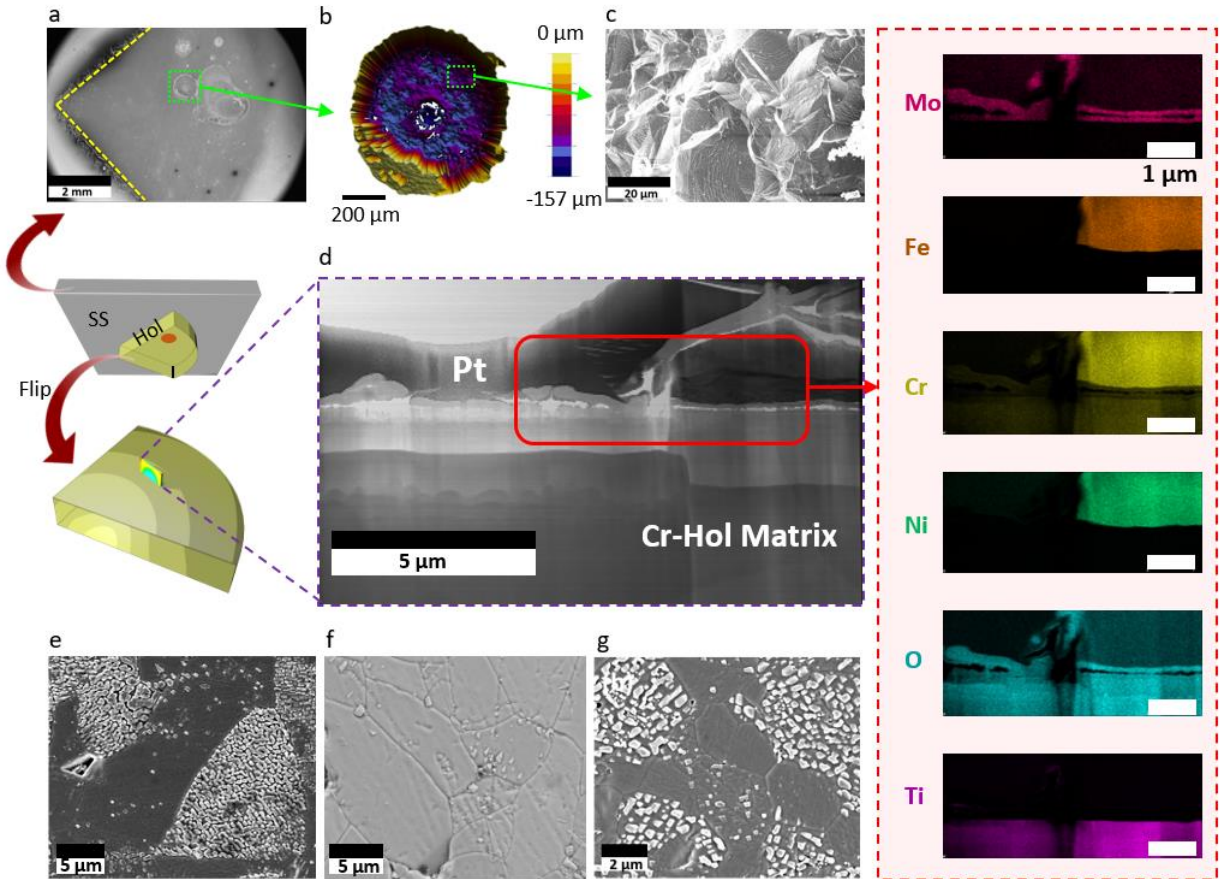


Fig. 5 Surface characterizations of SS and  $Ba_{1.15}Cr_{2.3}Ti_{5.7}O_{16}$  hollandite after corrosion. a) Localized corrosion on SS corroded in close proximity to  $Ba_{1.15}Cr_{2.3}Ti_{5.7}O_{16}$  hollandite in 0.6 M NaCl solution. The yellow dash lines indicate the boundary of the SS/Cr-Hol contact area. b) Three-dimensional topography of one large pit observed in the near center region of the crevice. c) The crystallographic pit morphology indicates that the pitting corrosion was under activation control. d) STEM-HAADF image and EDS elemental mapping for  $Ba_{1.15}Cr_{2.3}Ti_{5.7}O_{16}$  cross-section after corroded with SS for 28 days. This spot was selected near the center of the contact area, which was in contact with the large corrosion pit observed in b). The light and dark contrast in Cr-Hol matrix was caused by different thickness of the foil processed by FIB. e) Severe corrosion occurred in the crevice mouth area of  $Ba_{1.15}Cr_{2.3}Ti_{5.7}O_{16}$  after only 7 days. f) Less corrosion observed in the area between crevice mouth and center after 7 days. g) Morphology of  $Ba_{1.15}Cr_{2.3}Ti_{5.7}O_{16}$  corroded in HCl solution for 14 days.

Supplementary Materials for  
**Self-accelerated Corrosion of Nuclear Waste Forms at Material Interfaces**

Xiaolei Guo,<sup>1</sup> Stephane Gin,<sup>2</sup> Penghui Lei,<sup>3</sup> Tiankai Yao,<sup>3</sup> Hongshen Liu,<sup>4</sup> Dan K. Schreiber,<sup>5</sup> Dien Ngo,<sup>4</sup> Gopal Viswanathan,<sup>1</sup> Tianshu Li,<sup>1</sup> Seong H. Kim,<sup>4</sup> John D. Vienna,<sup>5</sup> Joseph V. Ryan,<sup>5</sup> Jincheng Du,<sup>6</sup> Jie Lian,<sup>3</sup> Gerald S. Frankel<sup>1\*</sup>

<sup>1</sup>*Department of Materials Science and Engineering, Ohio State University, Columbus, OH 43210, USA*

<sup>2</sup>*CEA, DEN, DE2D, SEVT, F-30207 Bagnols sur Cèze, France*

<sup>3</sup>*Department of Mechanical Aerospace and Nuclear Engineering, Rensselaer Polytechnic Institute, Troy, NY 12180*

<sup>4</sup>*Department of Chemical Engineering and Materials Research Institute, Pennsylvania State University, University Park, PA 16802, USA*

<sup>5</sup>*Energy and Environment Directorate, Pacific Northwest National Laboratory, Richland, WA 99352, USA*

<sup>6</sup>*Department of Materials Science and Engineering, University of North Texas, Denton, TX 76203, USA*

This file includes:

Supplementary Text

Table S1 to S5

Figs. S1 to S5

References

## Supplementary Text

### XPS characterization of corroded ISG and SS samples

XPS was used to obtain the elemental composition of corroded ISG samples. For each sample, three locations were investigated: edge of the ISG-SS316/PTFE contact area (crevice mouth), center of the contact area, and the non-contact area (back side of the contact area as a reference). The carbon-corrected elemental composition of corroded ISG was normalized to the concentration of Si for better comparison among different samples. Results are shown in Table S3 and plotted in **Fig 2e-2f**. Boron was depleted from the surface of all ISG samples, which is expected because boron is a mobile element that can rapidly leach out from the glass matrix via solvated ion diffusion<sup>1</sup>. For ISG that was in contact with PTFE, Na was only partially depleted from the surface, which was probably because the leaching solution contained a high concentration of Na<sup>+</sup> ions (0.6 M). The concentrations of Zr and Al were similar to that of the pristine glass. However, the Ca concentration was greatly reduced on both the contact and non-contact surfaces, suggesting ion exchange between Ca<sup>2+</sup> ions in the ISG and Na<sup>+</sup> ions in the solution.

Drastic changes in composition were identified on the ISG that was pressed against SS and corroded in 0.6 M NaCl solution. In the crevice mouth area, Na, Ca, Zr, and Al were all depleted from the surface, leaving behind a silica-like surface that was enriched in Fe. The observation is consistent with studies performed by Jain et al., who reported that 100% of the SRS 202G glass components except Si were released into the solution when the glass was exposed to 0.25 M FeCl<sub>3</sub> solution for 3 days<sup>2,3</sup>. The authors reported that the solution pH was as low as 1.1. It has been well documented that the pH within a crevice will drop upon the occurrence of metal crevice corrosion<sup>4,5</sup>, which is also due to the hydrolysis of metal cations. However, the actual electrolyte within a crevice could be much more aggressive than that employed by Jain et al., as the total concentration of metal cations including Fe<sup>2+</sup>, Cr<sup>3+</sup>, Ni<sup>3+</sup>, and Mo<sup>3+</sup> will increase until the solubility product of one of the metal hydroxides is reached<sup>4</sup>, which could be as high as several M<sup>6</sup>. Strong acidity will be created because of hydrolysis of these metal cations, which is likely the cause of corrosion damage observed on the ISG surface that was pressed against SS. In the center of the crevice, less Na, Al, and Zr was depleted from the surface compared to the crevice mouth regime, whereas the Ca concentration was similar to the pristine ISG. These results further demonstrated that when pressed against SS, the corrosion of glass was primarily localized in the crevice mouth area rather than spreading out homogeneously across the entire contact area, which is consistent with the visual observations presented in a previous section.

XPS was also used to characterize the SS sample that was pressed against ISG and corroded in 0.6 M NaCl at 90 °C for 30 days. The regions inside and outside of the crevice were both examined. The spectra

are shown in **Fig. 3e**. The Fe 2p spectra were fitted with a multiplex structure as shown in Fig. S4. A metallic iron peak was detected at 706.7 eV for both areas, indicating that the surface film was thinner than 10 nm. For the crevice area, Fe<sup>3+</sup> species were identified at 710.7 eV, which were likely Fe<sub>2</sub>O<sub>3</sub><sup>7</sup> that originated from the SS corrosion. It is unlikely that the Fe signals came solely from the SS passive film, as the Fe-bearing corrosion products were already identified on the ISG, so they should also exist on the SS surface that was in direct contact with ISG. The broad peak detected at 719.3 eV was characteristic of the shake-up satellite of Fe<sup>3+</sup> species<sup>8</sup>. However, for the area outside of the crevice, the peak position shifted toward lower binding energies. Deconvolution of the spectra suggests the existence of a new species located at 710.3 eV, which is likely associated with Fe-silicates<sup>9</sup>. The quantification of peak areas indicates that approximately 58% of Fe is present in the form of Fe<sub>2</sub>O<sub>3</sub> (710.7 eV), 6% is in metallic form (706.7 eV) that originated from SS substrate. The remaining 36% is in the form of Fe-silicates (710.3 eV). In addition, the Si 2p peak was centered at 102.6 eV for the crevice region (**Fig. 3e**). However, for the outside region, the Si 2p peak also shifted to a lower binding energy of 102.1 eV. The shift of both Fe 2p and Si 2p peaks to lower binding energies indicated that the Fe ions were incorporated into the silicate network<sup>8</sup>. In other words, a Fe-silicate film developed on the SS surface, which would likely consume silicates in the solution and the glass gel layer and thus accelerate glass corrosion.

### **Surface Roughness of as-abraded SS and ISG**

Optical profilometry was used to analyze the surface topography of as-abraded SS and ISG, which were abraded to 600 grit and 1200 grit, respectively. The average surface roughness (Ra) was calculated by Vision64 software. The Ra of SS calculated from three random locations was 0.3 μm, while the Ra for ISG was less than 0.1 μm. Therefore, the gap between the SS and ISG should be on the submicron scale. Crevice corrosion requires an occluded environment at the material interface, which means that the gap should be large enough for water molecules to enter, but it should also be small enough to limit mass transport. The threshold of this gap distance depends on various parameters, including the composition, passivity, and general corrosion resistance of the metals, and the aggressiveness of the environment such as temperature, pH, ionic strength, concentration of aggressive anions. It seems that surface roughness used in this study is sufficient to trigger crevice corrosion of SS under the testing conditions.

### **Chemical durability of hollandite**

The cumulative release of Cr or Al from hollandite was plotted as a function of time as shown in Fig. S5. It was found that proton concentration has a substantial impact on the leaching rate of both Cr-Hol and Al-Hol. In DI water, the leaching rate of Cr from Cr-Hol was quite low. When 0.01 M HCl was used as leachant, the overall dissolution kinetics increased by approximately 10 times, which was due to larger

number of sites being attacked by protons. For Al-Hol corroded in DI water, the initial release rate of Al for the first 5 h was approximately 40 mg/m<sup>2</sup>/h. When 0.01 M HCl was used, the initial release rate increased to 157 mg/m<sup>2</sup>/h. After 5 hours, the average leaching rate was also higher in 0.01 M HCl solution. Additionally, upon comparison of Al-Hol and Cr-Hol, it was found that the general release rate of Al from Al-Hol was significantly higher than the Cr release from Cr-Hol, which was independent of proton concentration, suggesting that the chemical durability of Cr-Hol is superior to Al-Hol. More results and the associated corrosion mechanisms will be discussed in a follow-up publication.

### Crevice corrosion models for SS/ISG and SS/Cr-Hol

Based on the corrosion results presented in the main text, the crevice corrosion morphologies on the metal side for SS/ISG and SS/Cr-Hol are different. The crevice corrosion of the SS in the SS/ISG system occurred along the periphery of the contacting area, i.e. the region of crevice mouth, while in the SS/Cr-Hol system, the crevice corrosion on the SS mainly took place in the interior part of the crevice. Furthermore, the corrosion attack was more severe in the SS/Cr-Hol system than in the SS/ISG system, as shown in **Fig. 2a** and **Fig. 5a**, respectively. The different corrosion morphologies on the metal side indicate that the interaction of interfaces for SS/ISG and SS/Cr-Hol (thus the mechanism of crevice corrosion) are different.

It is well known that the initiation and propagation of localized corrosion in metals depend on the temperature ( $T$ ), surface potential ( $E_{\text{surf}}$ ) and aggressiveness of the local environment, which can be represented by the concentration of metal cations at the corroded surface ( $C_{\text{surf}}$ )<sup>10,11</sup>.  $C_{\text{surf}}$  can be determined by the requirement of mass balance and Fick's first law of diffusion:

$$C_{\text{surf}} = \frac{i_{\text{met}} d_{\text{eff}}}{nFD} \quad \text{Eq. (1)}$$

where  $n$  is the average oxidation of state of the metal cations,  $F$  is the Faraday constant,  $D$  is the effective diffusion coefficient of metal cations in the localized environment,  $d_{\text{eff}}$  is the effective diffusion length of the metal cations, and  $i_{\text{met}}$  is the current density that describes the generation rate of metal cations by corrosion. For an alloy in the passive state,  $i_{\text{met}}$  can be considered to be the passive current density  $i_{\text{pass}}$ , while for active state,  $i_{\text{met}}$  represents the anodic dissolution current density. There exists a critical concentration of metal cations,  $C_{\text{crit}}$ , above which the passive film is not stable and the active dissolution can be sustained. Therefore, if  $C_{\text{surf}}$  in the entire crevice is larger than  $C_{\text{crit}}$ , active dissolution can occur on the whole surface, resulting in active corrosion in the crevice<sup>10,11</sup>. In contrast, if  $C_{\text{surf}}$  in the crevice is smaller than  $C_{\text{crit}}$ , extensive active dissolution will not occur but the pitting corrosion might occur at weak

points inside the crevice, and the crevice geometry outside the pit can accelerate and stabilize the pitting process.

For the SS/ISG crevice system, it was shown in the main text that a silicate film will precipitate on the alloy surface, acting as a barrier between the crevice solution and the alloy, thus greatly reducing the  $i_{\text{met}}$  for accumulation of metal cations. Under this condition, it is difficult for  $C_{\text{surf}}$  to reach the critical value of  $C_{\text{crit}}$  to initiate the extensive active dissolution inside the crevice. For a fixed temperature, the crevice corrosion is thereby dominated by  $E_{\text{surf}}$ , which is influenced by the ohmic potential ( $IR$ ) drop between the anode inside the crevice and the cathode outside the crevice. Because the  $IR$  drop between the anodic crevice and the cathode outside of the crevice is smallest at the crevice mouth, the local  $E_{\text{surf}}$  at the crevice mouth will be higher than the deeper region within the crevice. Therefore, the crevice corrosion on the metal side occurred primarily along the edge of the crevice, as shown in **Fig. 2a**. Such crevice corrosion should mainly initiate from pitting corrosion but is accelerated by the concentration and galvanic cell between the separated anode and cathode.

For the SS/Cr-Hol crevice system, there are two sources for the dissolved metal cations to initiate crevice corrosion: the passive dissolution of the SS and leaching of the Cr-Hollandite. Thus,  $i_{\text{met}}$  is the sum of the passive current density ( $i_{\text{pass}}$ ) and the effective leaching current density ( $i_{\text{leach}}$ ), i.e.  $i_{\text{met}} = i_{\text{pass}} + i_{\text{leach}}$ . According to Eq. 1, it is much easier for  $C_{\text{surf}}$  in the SS/Cr-Hol crevice system to reach the critical value of  $C_{\text{crit}}$ , especially at the center of the crevice, which has a large effective diffusion length  $d_{\text{eff}}$ . This perspective is supported by the observation of extensive active dissolution in the center area of the crevice, as shown in **Fig. 5a-5c**. The pitting corrosion observed near the crevice mouth is attributed to the small  $d_{\text{eff}}$ , which lowers  $C_{\text{surf}}$  on the metal surface below the  $C_{\text{crit}}$ , thus extensive active dissolution was inhibited, and only pitting corrosion can occur at some specific defective sites. The active dissolution morphology in the SS/Cr-Hol system indicated that the crevice corrosion was initiated by achieving  $C_{\text{crit}}$  across the metal surface, which was enhanced by the leaching process of Cr-Hol.

*Table S1 Nominal composition of ISG*

<b>As elements</b>	<b>Si</b>	<b>B</b>	<b>Na</b>	<b>Al</b>	<b>Ca</b>	<b>Zr</b>	<b>O</b>
<b>wt.%</b>	26.3	5.4	9.0	3.2	3.6	2.4	50.1

---

<b>As oxides</b>	<b>SiO<sub>2</sub></b>	<b>B<sub>2</sub>O<sub>3</sub></b>	<b>Na<sub>2</sub>O</b>	<b>Al<sub>2</sub>O<sub>3</sub></b>	<b>CaO</b>	<b>ZrO<sub>2</sub></b>
<b>mol%</b>	60.2	16.0	12.6	3.8	5.7	1.7

*Table S2 Nominal composition of SS316*

	<b>C</b>	<b>Mn</b>	<b>P</b>	<b>S</b>	<b>Si</b>	<b>Cr</b>	<b>Ni</b>	<b>Mo</b>	<b>N</b>	<b>Fe</b>
<b>wt.%</b>	<0.08	<2.00	<0.045	<0.030	<0.75	16.00 - 18.00	10.00 - 14.00	2.00 - 3.00	<0.10	Balance

*Table S3 Chemical composition of ISG surface that was corroded in close proximity to SS or PTFE in 0.6 M NaCl solution at 90 °C for 30 days. All compositions were normalized to Si*

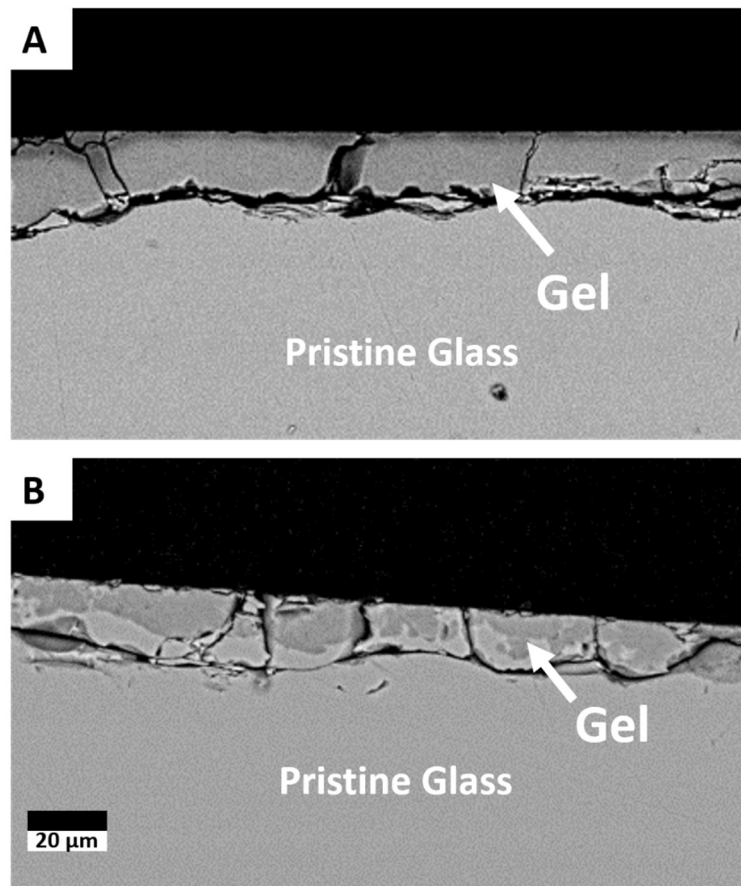
<b>Sample</b>	<b>Location</b>	<b>Na/Si</b>	<b>Ca/Si</b>	<b>Zr/Si</b>	<b>Al/Si</b>	<b>Fe/Si</b>
ISG(+SS)	Edge/Crevice Mouth	0.11	0.00	0.00	0.02	0.15
	Center of Crevice	0.17	0.13	0.03	0.08	0.09
	Back side/non-contact side	0.19	0.05	0.06	0.17	0
ISG(+PTFE)	Edge/Crevice Mouth	0.17	0.04	0.07	0.16	0
	Center of Crevice	0.17	0.01	0.04	0.12	0
	Back side/non-contact side	0.14	0.04	0.04	0.13	0
Pristine ISG	-	0.42	0.09	0.03	0.13	0

Table S4 List of experimental groups and testing conditions

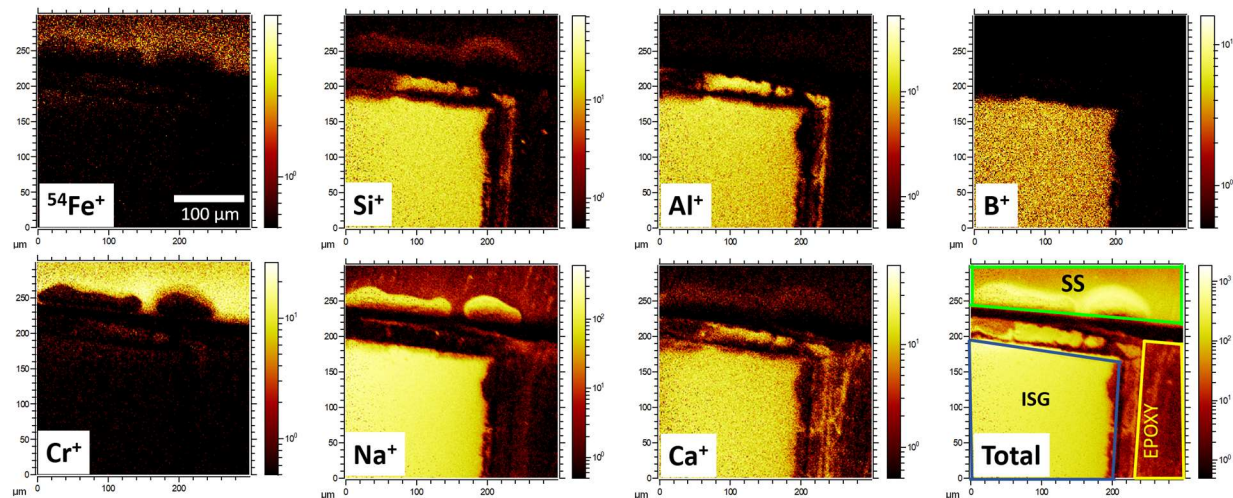
Sample ID	Materials	Solution	Temperature	Duration
ISG-SS-NaCl	ISG + SS 316	0.6 M NaCl	90 °C	30 Days
SS-PTFE-NaCl	SS 316 + PTFE	0.6 M NaCl	90 °C	30 Days
ISG-PTFE-NaCl	ISG + PTFE	0.6 M NaCl	90 °C	30 Days
Cr-Hol-SS-NaCl	Cr-Hol + SS 316	0.6 M NaCl	90 °C	7, 28 Days
Al-Hol-SS-NaCl	Al-Hol + PTFE	0.6 M NaCl	90 °C	7, 28 Days
Cr-Hol-HCl	Cr-Hol	0.01 M HCl	90 °C	Up to 14 Days
Al-Hol-HCl	Al-Hol	0.01 M HCl	90 °C	Up to 14 Days
Cr-Hol-DIW	Cr-Hol	DI water	90 °C	Up to 14 Days
Al-Hol-DIW	Al-Hol	DI water	90 °C	Up to 14 Days

Table S5 d spacing values extracted from diffraction patterns of needle-shaped phase with corresponding Miller indices

<i>d spacing</i> /Å	<i>Possible (h k l)</i>	<i>d spacing</i> /Å	<i>Possible (h k l)</i>
2.99	(-1 -3 2)	1.41	(-6 2 6)
2.79	(0 -3 2)	1.40	(-12 -4 1)
2.09	(-6 2 4)	1.38	(-12 -4 5)
1.87	(-8 5 2)	1.31	(-14 4 3)
1.83	(2 -6 -3), (-10 -1 1)	1.26	(8 8 1)
1.79	(-8 4 4)	1.24	(-4 8 5)
1.73	(-8 -6 2)	1.18	(2 12 0)
1.59	(-10 2 5)	1.16	(12 4 1)
1.49	(8 5 1)	1.15	(-10 9 5)



**Fig. S1** Cross-section images of A) ISG corroded in close proximity to SS in 0.6 M NaCl solution under 90 °C for 30 days. The maximum gel layer thickness was about 30 μm. B) ISG corroded in close proximity to PTFE in 0.6 M NaCl solution under 90 °C for 30 days. The maximum gel layer thickness was about 15 μm.



**Fig. S2** ToF-SIMS elemental mapping of the cross-section of epoxy mounted SS/ISG samples. A glass gel layer is visible at the interfaces between SS and ISG, as well as ISG and epoxy.

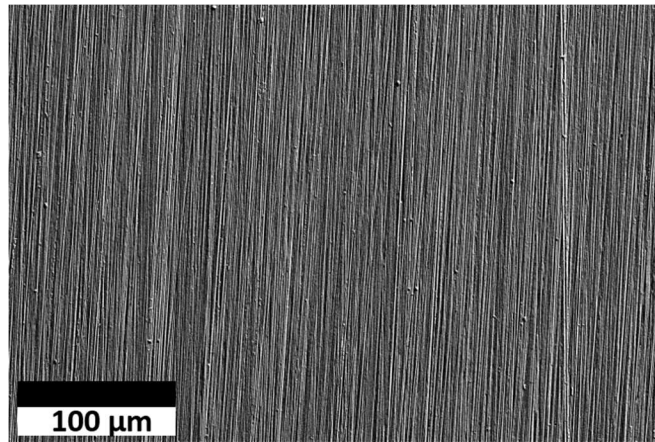


**Fig. S3** STEM/EDS analysis for the film precipitated on SS corroded in close proximity to ISG in 0.6 M NaCl solution at 90 °C for 30 days. A) HAADF image showing the cross-section of one particle being precipitated on the surface of SS. B) The film was located between the particle and SS substrate. C) The elemental mapping of the film.

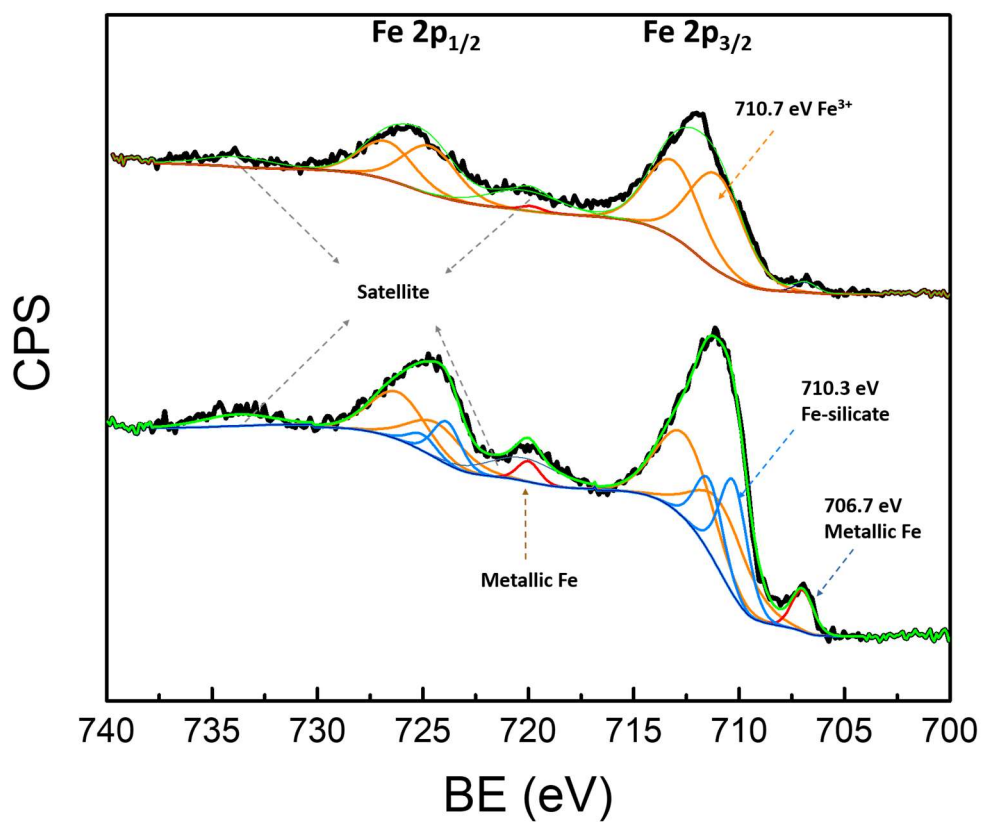


**Fig. S4** Fitted XPS spectra obtained from SS corroded in close proximity to ISG in 0.6 M NaCl solution. The areas inside and outside of the crevice are compared.

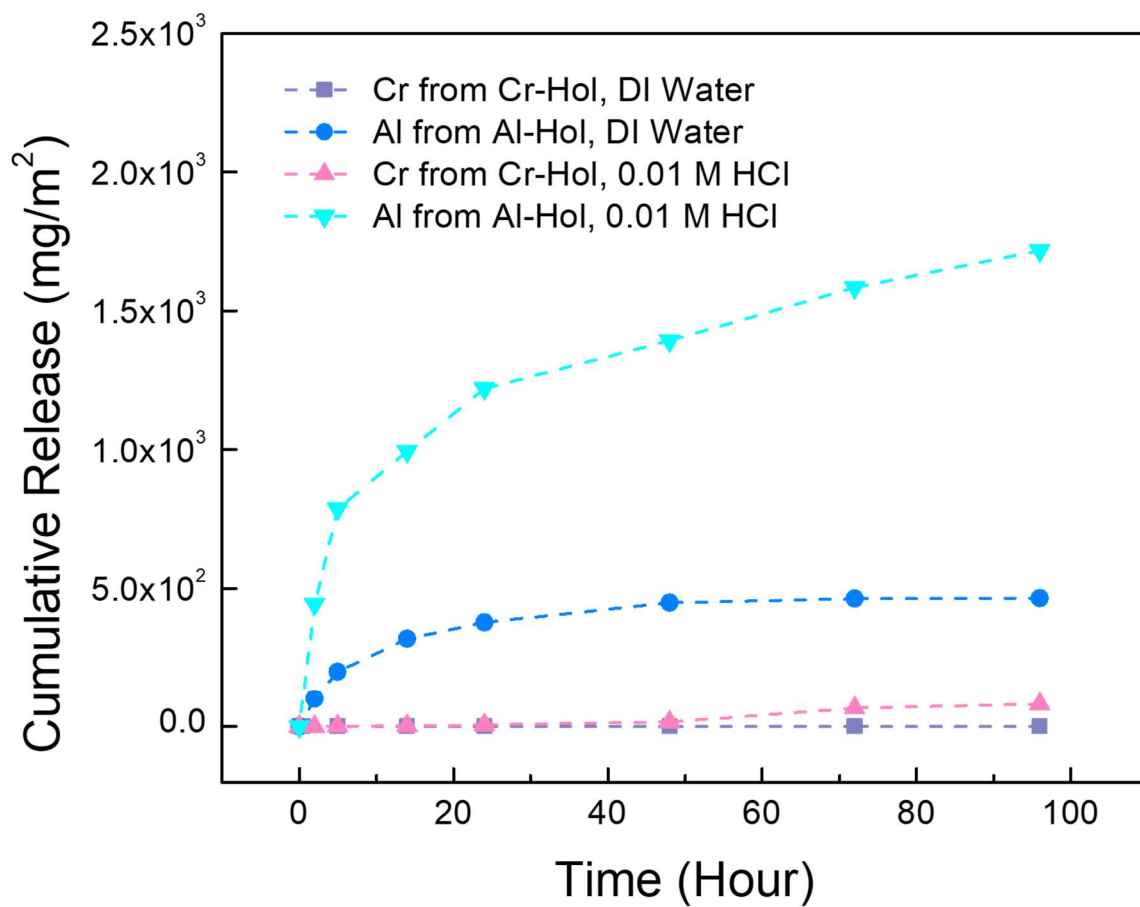


Fig. S5 Cumulative release of Cr and Al from Cr-Hol and Al-Hol, respectively.

## References

- 1 Frugier, P. *et al.* SON68 nuclear glass dissolution kinetics: Current state of knowledge and basis of the new GRAAL model. *J Nucl Mater* **380**, 8-21 (2008).
- 2 Jain, V. & Pan, Y. Performance of surrogate high-level waste glass in the presence of iron corrosion products. (Center for Nuclear Waste Regulatory Analyses, 2004).
- 3 Pan, Y.-M., Jain, V. & Pensado, O. Degradation of high-level waste glass under simulated repository conditions. *Journal of non-crystalline solids* **319**, 74-88 (2003).
- 4 Oldfield, J. & Sutton, W. Crevice corrosion of stainless steels: i. a mathematical model. *British corrosion journal* **13**, 13-22 (1978).
- 5 Kelly, R. G. in *Encyclopedia of Electrochemistry* (ed A. J. Bard) 275-307 (2007).
- 6 Oldfield, J. & Sutton, W. Crevice corrosion of stainless steels: II. Experimental studies. *British Corrosion Journal* **13**, 104-111 (1978).
- 7 Andersson, S. L. T. & Howe, R. F. An x-ray photoelectron study of metal clusters in zeolites. *The Journal of Physical Chemistry* **93**, 4913-4920, doi:10.1021/j100349a047 (1989).
- 8 Mekki, A., Holland, D., McConville, C. & Salim, M. An XPS study of iron sodium silicate glass surfaces. *Journal of non-crystalline solids* **208**, 267-276 (1996).
- 9 Seyama, H. & Soma, M. Fe 2p spectra of silicate minerals. *Journal of Electron Spectroscopy and Related Phenomena* **42**, 97-101, doi:https://doi.org/10.1016/0368-2048(87)85010-7 (1987).
- 10 Li, T., Scully, J. R. & Frankel, G. S. Localized Corrosion: Passive Film Breakdown vs Pit Growth Stability: Part II. A Model for Critical Pitting Temperature. *Journal of The Electrochemical Society* **165**, C484-C491, doi:10.1149/2.0591809jes (2018).
- 11 Li, T., Scully, J. R. & Frankel, G. S. Localized Corrosion: Passive Film Breakdown vs. Pit Growth Stability: Part III. A Unifying Set of Principal Parameters and Criteria for Pit Stabilization and Salt Film Formation. *Journal of The Electrochemical Society* **165**, C762-C770, doi:10.1149/2.0251811jes (2018).